A Distributed Ambient Backscatter MAC Protocol for Internet-of-Things Networks

Xuelin Cao, *Student Member, IEEE*, Zuxun Song, Bo Yang, *Member, IEEE*, Mohamed A. ElMossallamy, *Student Member, IEEE*, Lijun Qian, *Senior Member, IEEE*, and Zhu Han, *Fellow, IEEE*

***Abstract*—Ambient backscatter communication enabling device-to-device (D2D) communications via the ambient radio frequency (RF) signal has revealed its numerous application potential in the Internet-of-Things (IoT) networks. However, the work on the link layer for the backscatter communication is in its infancy due to the constraints of ultralow power and cost in such a system, especially a channel access protocol in the backscatter communication system for IoT networks is rarely mentioned. In this article, a distributed multiple access control (MAC) protocol is presented, which allows multiple backscatter devices (BDs) to connect with each other by relying on the ambient RF signal. By combining an analog channel sensing strategy with the dual-backoff mechanism, each BD can switch among the transmission, receiving, and energy harvesting (EH) states. Specifically, each BD starts a randomly designated time for EH once the channel is sensed to be busy. As the timer expires, the BD ceases the EH and continues its sensing and backoff procedures. With the consideration of the false alarm and the miss detection problems occurring while sensing, an enhanced 3-D Markov model is built to analyze the saturation throughput performance of the proposed MAC protocol. Extensive simulations verify the analysis and demonstrate the advantage of the proposed backscatter MAC protocol.**

***Index Terms*—Backscatter communications, Internet of Things (IoT), medium access control (MAC).**

I. Introduction

THE PROMISING Internet of Things (IoT) which focuses on green design, green production, green utilization, and green recycling has a great potential for life in the future (e.g., smart home, smart city, smart healthcare, smart grid, and industrial automation). To achieve the smart world sustainability, a continuous reduction of the energy consumption in IoT is necessary [1]. However, it is foreseen by the U.S. National Intelligence Council (NIC) that "by 2025, Internet nodes may exist in every daily thing, i.e., food packages, furniture, paper documents, etc.," the connectivity of tens of billions of network nodes will require more energy. Therefore, IoT toward low-power information and communications technologies [2] has been attracting numerous attention from academic, industry, and government. It is generally known that backscatter communications technologies have been implemented in the field of data-intensive wireless communications, such as device-to-device (D2D), cognitive radio (CR) [3]–[7], radio-frequency identification (RFID) [8]–[10], and IoT [11]–[13]. In particular, ambient backscatter communication is regarded as a promising solution for energy efficiency problems in the ultralow-power communications system likely IoT networks, where each smart device is able to transmit data by utilizing the ambient radio frequency (RF) sources [e.g., TV tower, FM tower, cellular base stations, Wi-Fi access points (APs), etc.] without requiring the active RF transmission. This capability enables backscatter communication as the last hop in the low-energy IoT with the features of low cost and ubiquitous deployment.

A. Motivations

Ambient backscatter communication is viewed as a significant development toward IoT due to its inherent features (e.g., low energy, low complexity, and low computation), however, there are still many key aspects to be studied, especially the multiple access control (MAC) protocol in such a system is in its infant stage. To date, most of the existing literature has adopted the centralized MAC protocol and has focused on a single backscatter device (BD) connection. As is well known, it might not be suitable to deploy the centralized MAC protocol into a large-scale IoT network only for sporadic backscatter communications requirement, which can be explained as well from the complexity, the energy consumption, and the dynamic change of network topology. It is therefore that how to coordinate the channel access among the BDs in a distributed manner is still an open problem. This motivates us to design a distributed MAC protocol relying on the backscatter

Manuscript received April 9, 2019; revised August 3, 2019, September 13, 2019, and November 2, 2019; accepted November 18, 2019. Date of publication November 26, 2019; date of current version February 11, 2020. This work was supported in part by the U.S. Multidisciplinary University Research Initiative (MURI) Air Force Office of Scientific Research (AFOSR) under Grant 18RT0073; in part by NSF Enhancing Access to the Radio Spectrum (EARS) under Grant 1839818; and in part by CNS under Grant 1717454, Grant 1731424, Grant 1702850, and Grant 1646607. *(Corresponding author: Xuelin Cao.)*

X. Cao and Z. Song are with the School of Electronics and Information, Northwestern Polytechnical University, Xi'an 710129, China (e-mail: caoxuelin@mail.nwpu.edu.cn; zxsong@nwpu.edu.cn).

B. Yang and L. Qian are with the Department of Electrical and Computer Engineering and the CREDIT Center, Prairie View A&M University, Texas A&M University System, Prairie View, TX 77446 USA (e-mail: boyang@pvamu.edu; liqian@pvamu.edu).

M. A. ElMossallamy is with the Department of Electrical and Computer Engineering, University of Houston, Houston, TX 77004 USA (e-mail: m.ali@ieee.org).

Z. Han is with the Department of Electrical and Computer Engineering, University of Houston, Houston, TX 77004 USA, and also with the Department of Computer Science and Engineering, Kyung Hee University, Seoul 446-701, South Korea (e-mail: zhan2@uh.edu).

Digital Object Identifier 10.1109/JIOT.2019.2955909

communications for IoT networks, which allows multiple BDs leveraging the ambient RF source to communicate with each other. In this article, one-hop communication with the same type of traffic as in the IoT network is taken into consideration. The challenges when we design the on-demand MAC protocol are threefold: 1) it should be designed to take into account the different types of ambient RF sources (i.e., the intermittent or continuous RF source signal); 2) it should have efficient power provision for backscatter transmission with the lower overhead; and 3) the collisions among BDs should be effectively avoided.

B. Contributions

Facing the aforementioned challenges, our contributions in this article can be summarized as follows.

1) An on-demand backscatter MAC protocol is proposed for the IoT networks, where the BDs can achieve power-efficient channel access via the RF signals according to its traffic requirements in a distributed way. Specifically, a system model considering the coexistence of the traditional RF communications and ambient backscatter communications is presented. On the one hand, the RF communication system consists of continuous RF source and the legacy RF users, and the RF sources not only provide RF communications but also generate the excitation signal to assist the backscatter communications. On the other hand, the backscatter communication system that relies on RF sources is constructed by a large number of BDs. Based on this model, the typical RF communication links, the backscatter communication links, and the interference links are distinguished accordingly. Different from the existing literature mainly focusing on the time-division-multiple access (TDMA) mode, where the frequency spectrum resources could be wasted and some critical data messages with high quality-of-service (QoS) can hardly be transmitted in time due to the inflexibility of the TDMA. In this article, each BD can compete the transmission opportunities based on its traffic demands dynamically in our proposed MAC protocol.
2) In the proposed backscatter MAC protocol, the energy harvesting (EH) is introduced into traditional carrier sense multiple access with the collision avoidance (CSMA/CA) backoff scheme, which is denoted as dual backoff. The proposed dual backoff contains two dimensions. The first-dimension backoff is to achieve collision avoidance and the second-dimension backoff aims to reduce the channel waste during the EH. Similar to the first-dimension backoff, there also exists a backoff counter δ for the second-dimension backoff, which is randomly chosen, i.e., $\delta \in [0, W_s - 1]$, where W_s denotes the contention window and $s \in [0, m]$ denotes the backoff stage. The two backoff counters of the dual-backoff scheme decrease simultaneously by one only if the current slot is idle. Once the channel becomes busy, the dual backoff hangs up and the BD can start to harvest energy. On the one hand, the harvested energy can be used to sense and the circuitry running on the chip. On the other hand, the communications between BDs are initiated using a backscatter mode. Besides, an analog channel sensing strategy combined with the dual-backoff mechanism is used to accomplish the effectively switching between the EH and the channel access.
3) A new state transition diagram is proposed where an EH state is introduced enabling the BDs to harvest energy dynamically. According to the proposed three states transition diagram, the BD can transit among the three states (i.e., "EH," "T," and "R" states). Furthermore, an algorithm illustrating the three-state transition in detail is presented, so as to make the proposed MAC protocol easier to follow. Note that the technical points above make this article different from the traditional CSMA/CA-based MAC and the existing backscatter MAC schemes. In contrast to the existed backscatter MAC protocols that build the connection between the reader and BDs, our MAC protocol can support the backscatter communications among BDs, and each BD can be viewed as a transmitter or a receiver.
4) Finally, an enhanced 3-D Markov model is developed to analyze the system throughput. Specifically, based on the existing 2-D backoff Markov model, one more dimension is introduced to indicate the backoff procedure for EH of each BD. With the proposed 3-D Markov model, the contention procedure of each BD can be characterized with the consideration of the sensing errors (i.e., false alarm and miss detection). Furthermore, the network throughput of the backscatter communication system is calculated, and then the optimal threshold is derived to maximize the system throughput. Extensive simulations are conducted using the network simulator (NS-2) to verify our analysis and demonstrate the superiority of the proposed dual-backoff scheme and the backscatter MAC protocol.

C. Related Works

Recently, some related works on the MAC protocol for the backscatter communication system have emerged. Specifically, to mitigate the interference among neighboring devices, the typical centralized mechanisms based on TDMA have been presented in [14]–[21]. By jointly leveraging the backscatter transmitter waveform and the maximum-likelihood detector in [14], the repeating structure of ambient orthogonal frequency-division multiplexing (OFDM) signals was exploited, which can be used to remove the direct-link interference of the backscatter receiver without increasing hardware complexity. Yang *et al.* [15] extended the work in [14] by designing a backscatter transmitter with multiantenna backscatter receivers. In [16], a full-duplex AP was designed to allow the simultaneously transmitting and receiving. Although the system performance is enhanced in [14]–[16], the computational complexity of these works is not suitable for the power-limited backscatter transceivers. Similar to [16], the full-duplex technology was also used in [17] and [18], whereas the main difference from [16] is that the multiple-access scheme is based on the time-hopping spread-spectrum (TH-SS), and this mechanism can realize

the full-duplex backscatter communications and simultaneous energy transfer in an interference network. However, this cannot be feasible for IoT networks due to the tremendous number of devices communicate with each other, and the other drawback is the large consumption of the spectrum bandwidth. In [19]–[21], backscatter communication were integrated with the CR network to improve the performance of the secondary system. However, the backscatter transmissions of the secondary users relying on the primary user's signal were performed based on time division, which led to a complicated time scheduling, and the secondary users could not accommodate to the changing of the network.

Different from the centralized MAC protocols, the slotted Aloha schemes with synchronization have been proposed as well for the backscatter communication system [22], [23]. For instance, an adaptive slotted Aloha protocol (ASAP) [22] was presented to reduce collisions by adjusting the frame size, but it required statistical information at the reader. To address this problem, preamble detection [i.e., utilizing clear channel assessment (CCA) to avoid collision] was introduced into the slotted Aloha [23], termed preamble sense multiple access (PSMA). In [24], by enabling perpetual sensing even at lower-level ambient power, collisions can be avoided and the MAC efficiency was improved. However, the collisions are still serious when two or more nodes start CCA by using the same backoff counter. Based on the preamble detection, several distributed MAC schemes for the backscatter communication system have been presented in [25]–[27]. In [27], energy detection was used to perform carrier sensing and arbitrate the channel state. In [25] and [26], enhancements including CTS_to_SELF transmission were proposed to confirm the association among multiple devices and reduce the collision. However, the association procedure may result in more power consumption. Similarly in [26], the Wi-Fi signal was also considered as the RF sources for IoT backscatter communications in [28], where Wi-Fi AP was allowed to separate Wi-Fi communications and backscatter communications, and each BD was enabled to complete the channel based on the CSMA/CA scheme. Since the communications of all BDs are constrained in a designated period, the competitions among BDs may incur serious collisions and bring more power consumption. In the replacement of Wi-Fi signal, the legacy cellular OFDM signal was employed to assist the backscatter communications in [29]. ElMossallamy *et al.* only solve the single BD communications without involving the channel access of multiple BDs.

The rest of this article is organized as follows. In Section II, the system model and preliminary backscatter communication works are presented. Section III describes the proposed distributed MAC protocol for ambient backscatter communications. Then, the throughput performance analysis is given in Section IV, followed by Section V providing some numerical results. Finally, we conclude this article in Section VI.

II. System Model and Preliminary Work

A. System Model

We consider a smart home scenario as shown in Fig. 1, where a co-existing system that consists of the legacy RF communications (i.e., the communications between the legacy RF user with RF sources) and the backscatter communications (i.e., the communications among BDs or the communications between the BD with the legacy RF user) is constructed, and each of them is defined as follows.

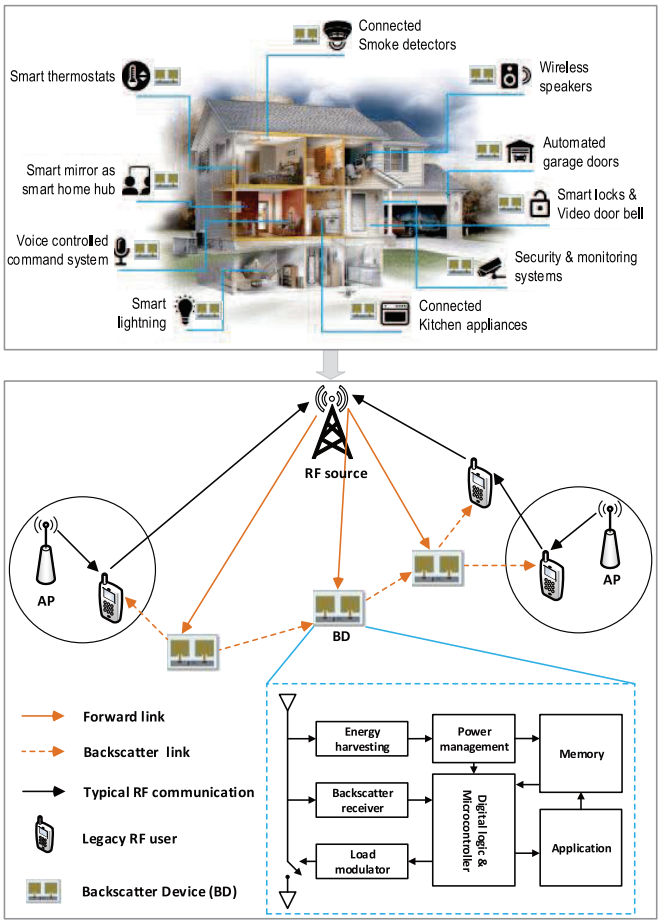

Fig. 1. System model.

Definition 1 (Legacy RF Communications):

1) *Legacy RF User:* A legacy RF user is capable of generating its RF transmission to communicate with the RF source.
2) *RF Communication Link:* It is designated as the wireless transmission link between the RF source and its dedicated legacy user.
3) *RF Interference Link:* It is the interference from one BD to the legacy user.

Definition 2 (Backscatter Communications):

1) *BD:* Compared to the legacy RF user, each BD is the semi-passive device that contains a backscatter antenna, a switched load impedance, a backscatter receiver, a micro-controller, a signal processor, an energy harvester, and other modules (e.g., memory and sensor). It leverages the harvested energy to support its sensing, circuitry running, and the backscatter communication that relying on RF signal.
2) *Backscatter Communication Link:* One backscatter communication link consists of a forward link (i.e., the wireless transmission link between RF source to the

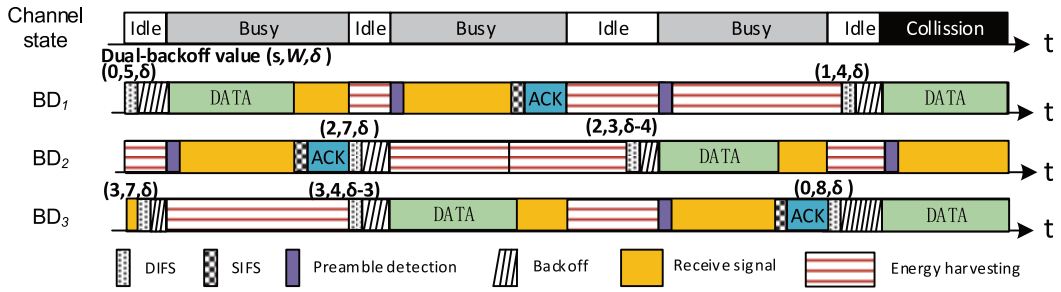

Fig. 2. Intuitional example of the backscatter transmission with three BDs.

BD transmitter) and a backscatter link (i.e., the wireless transmission link between the BD transmitter and the BD receiver); the backscatter link exists only when the forward link is active.

3) *Backscatter Interference Link:* The backscatter interference link refers to two types of links: one is the direct link, which draws the interference from the RF source to the BD receiver, and another one is the interference link, which belongs to the interference among BDs. Besides, we consider that the interference caused by the backscatter signal is generally with relatively low-power amplitude compared to the received RF signal, which is also verified by [27]. Therefore, the interference from the backscatter system is ignored because it is too weak to affect the conventional RF system.

In this article, we mainly consider the backscatter communications relying on a continuous RF signal. For the proposed system, $\mathbb{N} \triangleq (1, 2, \ldots, N)$ BDs are deployed. It is supposed that each semi-passive BD can perform EH from the existing continuous ambient RF source, e.g., TV tower, radio, cellular, etc. Moreover, the harvested energy can be stored to provide power for all modules of one BD. In addition, the connection between two BDs can be completed by backscattering, and with this mode, each BD can modulate the received ambient RF source signal by intentionally switching the load impedance to vary the amplitude and/or phase of its backscattered signal, and then the backscattered signal is received and finally decoded by its intended recipient.

With consideration of the multipath spread and the channel propagation delay, we denote $\mathcal{H} \triangleq (h_i | i \in \mathbb{N})$, $\mathcal{G} \triangleq (g_{ij} | i, j \in \mathbb{N}, i \neq j)$, and $\mathcal{F} \triangleq (f_j | j \in \mathbb{N})$ as the channel coefficients of forward links, backscatter links, and direct links, respectively. Here, $\mathcal{H}$, $\mathcal{F}$, and $\mathcal{G}$ are considered as circularly symmetric complex Gaussian (CSCG) random variables with mean zero and variance of $\mathbb{E}[|h_i|^2] = \sigma_{h_i}^2$, $\mathbb{E}[|f_j|^2] = \sigma_{f_i}^2$, and $\mathbb{E}[|g_{ij}|^2] = \sigma_{g_{ij}}^2$, respectively. We further assume that the interference from each BD to the legacy user can be neglected since the backscatter signals are too weak to affect the RF legacy users' communications.

B. Preliminary Work of Backscatter Communications

Based on the proposed system model, we figure out the operation of backscatter communications. Denote the ambient RF source signal as $s(n)$, and then let the backscatter signal of the ith BD be $b_i(n)$. When the ith BD connects its intended recipient by backscattering the RF source signal, it is assumed that the received signal is sampled on $s(n)$ at the Nyquist rate, and the number of the transmitted symbol by the ith BD is L. We further assume that the adjacent samples in the $s(n)$ are independent and identically distributed.

For the backscatter communications, once receiving the RF source signal through the forward link, the backscatter signal $b_i(n)$ is transmitted by the ith BD to its intended recipient (i.e., the jth BD) can be given as

$$b_i(n) = \eta_i h_i B_i^k(n) s(n), \qquad B_i^k(n) = \{0, 1\} \tag{1}$$

where $i \in \mathbb{N}$, $n = (k-1)M + 1, \ldots, kM$, $k \in [1, L]$, M is the received samples. η_i is the complex attenuation of the backscattered signal from the ith BD. $B_i^k(n)$ is the kth symbol that is transmitted by the ith BD, which equals to 0 or 1. Since the samples are uncorrelated, if BD conveys information with $1/M$ sampling rate, then $B_i^k(n)$ are identical for $n = (k-1)M + 1, \ldots, kM$, $k \in [1, L]$, i.e., $B_i^k(n) = B_i^k$. It is known that the RF source signal $s(n)$ follows the circularly symmetric complex Gaussian distribution. Thus, after the backscatter link, the received backscatter signal samples at the intended recipient is $g_{ij} b_i(n)$, $i, j \in \mathbb{N}$, $i \neq j$.

Considering the backscatter interference links, which come from RF source and the other BDs, i.e., the direct signal from RF source is denoted as $f_j s(n)$, and the interference signals $I(n)$ from other BDs can be expressed as

$$I(n) = \sum_{l=1, l \neq i}^{N} g_{lj} \eta_l h_l B_l s(n), \qquad B_l = \{0, 1\} \tag{2}$$

where $l \in \mathbb{N}$, $l \neq i$, η_l is the complex attenuation of backscattered signals from the lth BD. B_l takes a value of "0" or "1" depending on the lth BD is nonreflecting or reflecting state. When $I(n) = 0$, it means that $B_l = 0$ $\forall l \neq i \in \mathbb{N}$, i.e., all of nearby BDs are nonreflecting states. In contrast, $I(n) \neq 0$ can be explained that $B_l = 1, \exists l \neq i \in \mathbb{N}$, i.e., at least one nearby BD is reflecting state.

Thus, the received signals at the intended recipient $y_j(n)$ can be expressed as

$$y_j(n) = f_j s(n) + g_{ij} b_i(n) + I(n) + w_j(n) \tag{3}$$

where $i, j, l \in \mathbb{N}$, $i \neq j \neq l$, $n = (k-1)M + 1, \ldots, kM$, $k \in [1, L]$, $w_j(n) \backsim \mathcal{CN}(0, N_{w_j})$ is the additive white Gaussian noise (AWGN).

Let $\mu_i = \eta_i g_{ij} h_i$ and $\mu_l = \eta_l g_{lj} h_l$, respectively. For simplicity, the noise signal in (3) can be neglected, and then the received signals at the jth BD can be rewritten as

$$y_j(n) = \begin{cases} f_j s(n) + I(n), & B_i^k = 0 \\ f_j s(n) + \mu_i s(n) + I(n), & B_i^k = 1. \end{cases} \tag{4}$$

It should be noted that in the scenes of multiple backscatter communication links, to distinguish the received interference backscatter signals at the intended recipient, we consider the following two cases.

1) $B_i^k = 0, \exists i \in \mathbb{N}$, i.e., the ith BD is nonreflecting state. In this case, the received signal at the receiver contains the interference backscatter signals or not, which is given as

$$y_j^0(n) = \begin{cases} f_j s(n), & I(n) = 0 \\ f_j s(n) + I(n), & I(n) \neq 0. \end{cases} \tag{5}$$

2) $B_i^k = 1, \exists i \in \mathbb{N}$, i.e., the ith BD is reflecting state. In this case, the received signal at the receiver contains the interference backscatter signals or not, which is given as

$$y_j^1(n) = \begin{cases} f_j s(n) + \mu_i s(n), & I(n) = 0 \\ f_j s(n) + \mu_i s(n) + I(n), & I(n) \neq 0. \end{cases} \tag{6}$$

Then, the average received power in the M received samples corresponding to a single backscattered symbol (i.e., the kth symbol) at the intended recipient can be presented as

$$\mathbb{P}_i = \frac{1}{M} \sum_{n=(k-1)M+1}^{kM} |y_j(n)|^2, \quad k \in [1, L]. \tag{7}$$

Submitting (5) and (6) into (7), we have

$$P_j^0 = \begin{cases} |f_j|^2 \mathbb{P}_s, & I(n) = 0 \\ |f_j + \sum_{l=1, l\neq i}^{N} \mu_l B_l|^2 \mathbb{P}_s, & I(n) \neq 0 \end{cases} \tag{8}$$

and

$$P_j^1 = \begin{cases} |f_j + \mu_i|^2 \mathbb{P}_s, & I(n) = 0 \\ |f_j + \mu_i + \sum_{l=1, l\neq i}^{N} \mu_l B_l|^2 \mathbb{P}_s, & I(n) \neq 0 \end{cases} \tag{9}$$

where $i, j, l \in \mathbb{N}, i \neq j \neq l$. B_l equals 0 or 1, $\mathbb{P}_s$ is the average power of the received RF signal, and it is denoted as

$$\mathbb{P}_s = \frac{1}{M} \sum_{(k-1)M+1}^{kM} |s(n)|^2. \tag{10}$$

III. Proposed Backscatter MAC Protocol

A. Basic Idea and Packet Format

1) Key Idea: The proposed distributed backscatter MAC protocol mainly differs from the existing works in the following three ways. An intuitional example of the proposed backscatter MAC protocol is shown in Fig. 2, where three BDs (denoted as BD_1, BD_2, and BD_3) are deployed to coordinate channel access in a distributed way.

1) *Three-State Transition:* Considering the hardware constraint of a BD[1] and the time-switching architecture (i.e., duty cycle) being generally implemented in the BD prototype in practical scenarios [24], [27], [31], EH is a critical issue to be resolved in backscatter communications. In this article, to resolve this issue, each BD is assumed to maintain three states: 1) EH (including "Harvesting" substate and "Sensing" substate); 2) "T" (including "Backoff" substate and "Send" substate); and 3) "R," as illustrated in Fig. 3. In particular, the harvested energy at the Harvesting substate can be used to power the sensors and the digital logic units (e.g., microcontroller), and to provide the small amounts of power required for ambient backscatter communication or the required power for typical RF communication, especially when the ambient signal strength is weak or even unavailable. The three-state transition is described in Section III-B in detail.

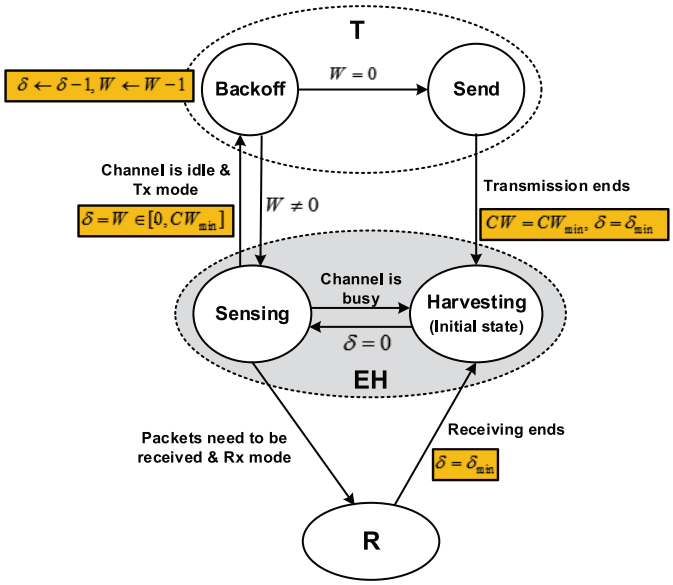

Fig. 3. State transition diagram.

2) *Dual-Backoff Scheme:* We introduce the EH into the traditional CSMA/CA backoff procedure, which is denoted as dual backoff. The proposed dual backoff contains two dimensions. The first-dimension backoff is to achieve collision avoidance and the second-dimension backoff aims to reduce the channel resources waste during the EH. Specifically, in our proposed MAC protocol, if the channel is sensed to be busy, the transmitting BD starts EH according to a preset timer δ. When the channel becomes idle, the BD continues to decrease both the backoff counters of the two dimensions backoff procedure. However, if δ is fixed or randomly selected (i.e., the second-dimension backoff is not used), the BD usually spends more time on the EH before the data transmission, even if the channel has already become idle. The dual-backoff scheme is detailed in Section III-C.

3) *Sensing Mechanism:* Since the power of BD in the backscatter communication system is limited, an ultralow-power consumed sensing strategy is reasonably adopted during the procedure of backoff, i.e., each BD performs channel sensing according to the analog circuit [27], which is instead of traditional energy detection.

[1]The BD generally consists of a transmitter, a receiver, and a harvester, which operate independently of each other [27].

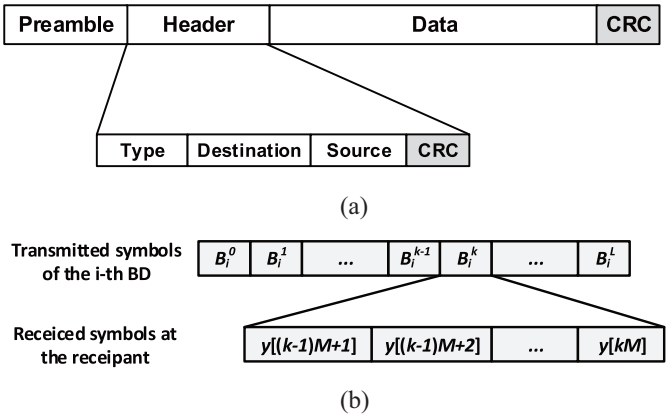

Fig. 4. (a) Packet format and (b) symbols transmission.

By using an analog comparator and compare the averaged signal to a given threshold, the channel state can be detected. More details are given in Section III-D.

2) Packet Format: Fig. 4(a) illustrates the packet format for the backscatter communication system. The packet begins with the preamble that contains 1 and 0 bits information, which can be used by the BD to judge itself whether it is the intended receiver. The preamble is followed by a header, which specifies some information, such as the type of packet, the destination address, and the source of the packet. Following the data payload, a CRC in both of the header and data is used to detect bit errors. Fig. 4(b) shows the symbols transmission, where $B_i^k \in \{0, 1\}$ denotes the kth binary symbol of the ith BD transmitter. Each symbol has an equal probability of being 0 and 1 due to the random characters coding as well as interleaving.

B. Three-State Transition

We further clarify the procedure of the three-state transition, as presented in Algorithm 1. For clarity, we describe the state transition procedure in the following two aspects according to the working mode of the BDs, i.e., the "Tx" mode or "Rx" mode depending on the data packets accumulated in the MAC queue. That is to say, if there exist data packets in the MAC queue, the working mode of the BD is Tx. Otherwise, the working mode of the BD is Rx.

1) *The BD Works at the Tx Mode Diagram:* This means that there exist data packets to be transmitted in the MAC queue. Initially, the BD stays at the Harvesting substate with a preset timer, i.e., $\delta = \delta_{\min}$, where $\delta_{\min}$ can be determined by the BDs themselves. The BD stays at the Harvesting substate and harvests energy for the time duration of $\delta\sigma$, where σ denotes the duration of a time slot. When the time counter δ decreases to be 0, the BD switches to the Sensing substate and performs the channel sensing. If channel is sensed to be idle within a time slot, then the BD switches to the Backoff substate and decreases the backoff counter and δ by 1, i.e., $W \leftarrow W - 1, \delta \leftarrow \delta - 1$, where $\delta = W \in [0, \mathrm{CW}_{\min}]$. If the backoff counter W is not decreased to 0 yet, then the BD switches back to the Sensing substate and continues to perform the channel sensing. Otherwise, i.e., $W = 0$ holds, then the BD switches to the Send substate. After the transmission ends, the BD switches back to the Harvesting substate and set $\mathrm{CW} = \mathrm{CW}_{\min}$ and $\delta = \delta_{\min}$.

2) *The BD Works at the Rx Mode:* This means that there are no data packets to be transmitted in the MAC queue. As illustrated in Fig. 3, the BD first switches to the Sensing substate when $\delta = 0$ is satisfied. Then, once it detects that there exist data packets to be received, the BD switches from Sensing substate to the R state and receives the data packets accordingly. When the packets receiving is finished, the BD switches back to the Harvesting substate and set $\delta = \delta_{\min}$.

Algorithm 1 Three States Transition Algorithm

Require: Three states (i.e., 'EH', 'T' and 'R') are maintained by the deployed BDs, and each BD can freely switch among these three states
Initialize state of the deployed BDs as "Harvesting" of "EH" state
if The BD has the data transmission request (i.e., the BD works at the Tx mode), **then**
  Switches into the "Sensing" sub-state and sets the state variables as (s, W, δ)
  Performs the analog channel sensing
  if channel is idle in the current time slot, **then**
    $W \rightarrow W - 1$, $\delta \rightarrow \delta - 1$ (i.e., the dual-backoff operation)
    if $W \neq 0$ **then**
      The BD switches to the "Sensing" sub-state and continues to perform channel sensing in the next time slot
    else
      The BD switches into the 'Send' state and transmits data
    end if
  else
    The BD ceases the backoff procedure and switches into the "Harvesting" sub-state for the duration of $\sigma\delta$, where σ is the duration of one slot
  end if
  After finishing the transmission, the BD switches into the "Harvesting" sub-state and resets $\delta = \delta_{min}$, $CW = CW_{min}$
else
  There is no traffic request (i.e., the BD works at the Tx mode)
  Switches to the "Sensing" sub-state if $\delta = 0$
  Performs the preamble detection to detect the packet from the channel
  if Yes, **then**
    Switches into 'R' state
    if The destination of the data packet is the BD itself, **then**
      The BD receives the data packet
    else
      The BD goes back into its "Harvesting" sub-state and resets $\delta = \delta_{min}$
    end if
  else
    Switches back to the "Harvesting" sub-state
  end if
end if

C. Dual-Backoff Mechanism

As well as we knew, the typical binary exponential backoff scheme is adopted in IEEE 802.11 DCF. Based on this, a novel dual-backoff mechanism is presented in our proposed MAC protocol, where an additional backoff scheme is introduced

into the EH to improve the channel utilization. Specifically, after a period of time called DCF interframe space (DIFS), the requested BD first sets its backoff value (s, W, δ) and starts the backoff procedure, where $W \in [0, W_s - 1]$ and $s \in [0, m]$ denote as the value of backoff counter and the backoff stage, respectively, that belongs to the first-dimension backoff. Besides, $\delta = W$ is the time of EH which represents the second-dimension backoff. Here, W_0 and W_m represent the minimum contention window and the maximum contention window, m is the maximum backoff stage. Next, the required BD senses the channel state by adopting the sensing scheme which has been mentioned in Section III-D. Once the channel is sensed to be idle, the BD decreases the value of W and δ by one after a slot, i.e., $W = W - 1$ and $\delta = \delta - 1$. Otherwise, if the channel is sensed to be busy, the backoff procedure is suspended, the required BD performs EH and stores the energy with using EH technologies [32]–[35]. Once the preset timer δ periods out, the required BD continues its backoff if the channel is sensed to be idle until the backoff counter W becomes zero. That means the backoff value of the dual-backoff scheme can be dynamically adjusted with the network changing, thereby avoiding competition collisions and reducing the time overhead. Note that the harvested energy can be used to perform channel sensing, receiving packets, and even transmitting when the ambient signal is weak or unavailable.

D. Analog Channel Sensing

The channel sensing is performed based on energy detection by leveraging the proposed analog comparator in [27]. Each BD determines signal changes through the analog comparator's minimum threshold. Specifically, in the absence of a nearby BD transmission, the comparator outputs either a sequence of 1 or a sequence of 0 since it does not record any changes below the threshold. In the presence of a nearby BD transmission, on the other hand, results in changes that are greater than the threshold and therefore the same number of 1 and 0 at the comparator's output.

Concretely, let ϕ denote as the sensing statistics result, energy detection is depicted as the following equation:

$$\phi = 1 - \frac{|N^0 - N^1|}{N^0 + N^1} \tag{11}$$

where N^0 and N^1 denote the number of 0 and 1, respectively, which can be observed at the BD's comparator over some time intervals. In the presence of a nearby BD, the average number of 0 and 1 is nearly the same, and hence ϕ is close to one. Conversely, in the absence of any nearby BDs, the bits output by the comparator are either mostly 1 or mostly 0, thus ϕ is close to zero.

IV. Performance Analysis

In this section, we first discuss two sensing problems in the backscatter communication system, i.e., the false alarm and the miss detection. Moreover, an enhanced 3-D discrete Markov model is drawn with considering the probability of false alarm and miss detection. According to the 3-D Markov model, the throughput performance of the proposed MAC protocol for backscatter communications is analyzed, and the throughput upper bound is achieved as well with an optimal threshold.

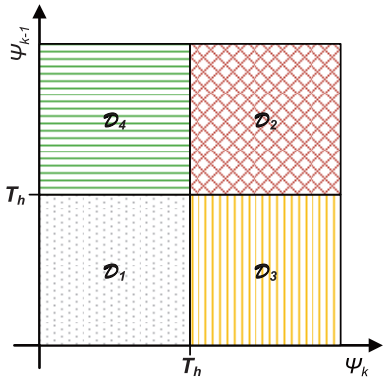

Fig. 5. Decision region.

A. Sensing Errors

Once the ith BD has the backscatter transmission request, the channel sensing is first performed by checking the test statistics ψ_k, which is shown as

$$\psi_k = \sum_{n=(k-1)M+1}^{kM} \left| f_i + \sum_{l=1, l\neq i}^{N} \mu_l B_l \right|^2 |s(n)|^2 \tag{12}$$

where $i, l \in \mathbb{N}, i \neq l, k \in [1, L]$. Intuitively, ψ_k statistically keeps two different levels when the nearby lth BD is in the nonreflecting state and the reflecting state, which can be used for general energy detection. However, in order to reduce the power consumption, an analog channel sensing scheme which uses a comparison circuit replacement of the ADC [27] is adopted. Since a threshold (T_h) exists in the analog comparator, the averaging circuit smoothens out the variations of the ambient signals. Specifically, the one input of the analog comparator is the output of the average envelope circuit, and the other input of the analog comparator is the threshold value, T_h. By comparing these two inputs, each BD can distinguish the presence and absence of a nearby BD. In other words, the interference information can be obtained according to the sensing statistics result, ϕ, i.e., if the value of ϕ equals to zero, it means the absence of a nearby BD, otherwise, the presence of a nearby BD is determined.

To confirm ϕ, the difference is observed between adjacent signals to check whether there is a significant change at the comparator (whether or not existing the different number of 1 and 0). For a given threshold T_h, jointly utilize the two energies, ψ_k and ψ_{k-1}, and then the four decision regions can be presented by $\mathcal{D}_1, \mathcal{D}_2, \mathcal{D}_3$, and $\mathcal{D}_4$, which are shown in Fig. 5. Thus, the decision procedure of ϕ can be described as follows:

$$\phi = \begin{cases} 0, & \mathcal{D}_1 \ (\psi_{k-1} \leq T_h, \quad \psi_k \leq T_h) \\ 0, & \mathcal{D}_2 \ (\psi_{k-1} > T_h, \quad \psi_k > T_h) \\ 1, & \mathcal{D}_3 \ (\psi_{k-1} \leq T_h, \quad \psi_k > T_h) \\ 1, & \mathcal{D}_4 \ (\psi_{k-1} > T_h, \quad \psi_k \leq T_h) \end{cases} \quad \forall k \in [1, L]. \tag{13}$$

Based on (13), if $\phi = 0$, it indicates there is no change between adjacent signals, i.e., the absence of a nearby BD is judged,

otherwise, the presence of a nearby BD is determined. It is noted that each BD can directly make a fast decision according to the value of ϕ with low complexity. Clearly, the threshold T_h should be designed appropriately in order to guarantee reliable sensing results.

Let $\mathfrak{H}_0$ and $\mathfrak{H}_1$ represent the hypotheses that all nearby BDs keep silent and at least one nearby BD is active, respectively. Given this fact, two errors will be introduced when the channel sensing beginning, i.e., the false alarm and the miss detection.

1) The ith BD makes a decision that $\psi_{k-1} \le T_h, \psi_k > T_h$ or $\psi_{k-1} > T_h, \psi_k \le T_h$ when all nearby BDs are in the nonreflecting state, i.e., $B_l = 0\ \forall l \in \mathbb{N} and l \ne i$. In this case, the false alarm appears, and the probability of false alarm can be expressed as

$$p_f = P(\phi = 1|\mathfrak{H}_0). \tag{14}$$

2) The ith BD makes a decision that $\psi_{k-1} \le T_h, \psi_k \le T_h$ or $\psi_{k-1} > T_h, \psi_k > T_h$ when at least one nearby BD is in the reflecting state, i.e., $B_l = 1, \exists l \in \mathbb{N},$ and $l \ne i$. In this case, the miss detection appears, and the probability of miss detection can be expressed as

$$p_m = P(\phi = 0|\mathfrak{H}_1). \tag{15}$$

Combining (13) with (14) and (15), we have

$$p_f = P(\phi = 1|\mathfrak{H}_0) = \frac{1}{2}P(\mathcal{D}_3|\mathfrak{H}_0) + \frac{1}{2}P(\mathcal{D}_4|\mathfrak{H}_0) \tag{16}$$

and

$$p_m = P(\phi = 0|\mathfrak{H}_1) = \frac{1}{2}P(\mathcal{D}_1|\mathfrak{H}_1) + \frac{1}{2}P(\mathcal{D}_2|\mathfrak{H}_1). \tag{17}$$

Let $P(\mathcal{D}_\beta|\mathfrak{H}_\alpha), (\alpha = 0, 1; \beta = 1, 2, 3, 4))$ be the probability of making region decision $\mathcal{D}_\beta$ under the hypothesis of $\mathfrak{H}_\alpha$, and then we can obtain

$$\begin{cases} P(\mathcal{D}_1|\mathfrak{H}_0) = P(\psi_{k-1}|\mathfrak{H}_0 \le T_h, \psi_k|\mathfrak{H}_0 \le T_h) \\ P(\mathcal{D}_2|\mathfrak{H}_0) = P(\psi_{k-1}|\mathfrak{H}_0 > T_h, \psi_k|\mathfrak{H}_0 > T_h) \\ P(\mathcal{D}_3|\mathfrak{H}_0) = P(\psi_{k-1}|\mathfrak{H}_0 \le T_h, \psi_k|\mathfrak{H}_0 > T_h) \\ P(\mathcal{D}_4|\mathfrak{H}_0) = P(\psi_{k-1}|\mathfrak{H}_0 > T_h, \psi_k|\mathfrak{H}_0 \le T_h) \\ P(\mathcal{D}_1|\mathfrak{H}_1) = P(\psi_{k-1}|\mathfrak{H}_1 \le T_h, \psi_k|\mathfrak{H}_1 \le T_h) \\ P(\mathcal{D}_2|\mathfrak{H}_1) = P(\psi_{k-1}|\mathfrak{H}_1 > T_h, \psi_k|\mathfrak{H}_1 > T_h) \\ P(\mathcal{D}_3|\mathfrak{H}_1) = P(\psi_{k-1}|\mathfrak{H}_1 \le T_h, \psi_k|\mathfrak{H}_1 > T_h) \\ P(\mathcal{D}_4|\mathfrak{H}_1) = P(\psi_{k-1}|\mathfrak{H}_1 > T_h, \psi_k|\mathfrak{H}_1 \le T_h). \end{cases} \tag{18}$$

Let Λ_α and $1 - \Lambda_\alpha$ be defined as

$$\Lambda_\alpha = P(\psi_k|\mathfrak{H}_\alpha > T_h), \qquad \alpha = 0, 1 \tag{19}$$

and

$$1 - \Lambda_\alpha = P(\psi_k|\mathfrak{H}_\alpha \le T_h), \quad \alpha = 0, 1. \tag{20}$$

Then, (18) can be rewritten as

$$\begin{cases} P(\mathcal{D}_1|\mathfrak{H}_0) = (1 - \Lambda_0)^2 \\ P(\mathcal{D}_2|\mathfrak{H}_0) = \Lambda_0^2 \\ P(\mathcal{D}_3|\mathfrak{H}_0) = (1 - \Lambda_0)\Lambda_0 \\ P(\mathcal{D}_4|\mathfrak{H}_0) = \Lambda_0(1 - \Lambda_0) \\ P(\mathcal{D}_1|\mathfrak{H}_1) = (1 - \Lambda_1)^2 \\ P(\mathcal{D}_2|\mathfrak{H}_1) = \Lambda_1^2 \\ P(\mathcal{D}_3|\mathfrak{H}_1) = (1 - \Lambda_1)\Lambda_1 \\ P(\mathcal{D}_4|\mathfrak{H}_1) = \Lambda_1(1 - \Lambda_1). \end{cases} \tag{21}$$

Consider the modeling and performance analysis of the backscatter communication system that operates over Rayleigh fading channels [36]. From (12), $|f_i + \sum_{l=1, l\ne i}^{N} \mu_l B_l|^2$ can be regarded the Chi-squared (χ^2) distributed with M degrees of freedom. Therefore, ψ_k follows the gamma distribution, the probability density function (PDF) of which can be given as

$$f_\psi(x) = \frac{x^{M-1}e^{-\frac{x}{\theta_\alpha}}}{\theta_\alpha^M \Gamma(M)} \tag{22}$$

where $\Gamma(x) = \int_0^\infty e^{-t}t^{x-1}dt$ is a gamma function. Besides, θ_α can be valued as

$$\theta_\alpha = \begin{cases} \sigma_{f_i}^2 \mathbb{P}_s, & \alpha = 0 \\ \left(\sigma_{f_i}^2 + \sum_{l=1, l\ne i}^{N} \eta_l^2 g_{li}^2 \sigma_{h_l}^2\right)\mathbb{P}_s, & \alpha = 1. \end{cases} \tag{23}$$

Hence, $\Lambda_\alpha, \alpha \in \{0, 1\}$ can be obtained as

$$\Lambda_0 = P(\psi_k|\mathfrak{H}_0 > T_h) = \Gamma\left(M, \frac{T_h}{\theta_0}\right) \tag{24}$$

and

$$\Lambda_1 = P(\psi_k|\mathfrak{H}_1 > T_h) = \Gamma\left(M, \frac{T_h}{\theta_1}\right) \tag{25}$$

where $\Gamma(a, x)$ is the incomplete gamma function given by $\Gamma(a, x) = (1/\Gamma(a)) \int_0^x t^{a-1}e^{-t}dt$.

Substituting (21), (24), and (25) into (16) and (17), p_f and p_m can be calculated as

$$\begin{aligned} p_f &= (1 - \Lambda_0)\Lambda_0 \\ &= \left(1 - \Gamma\left(M, \frac{T_h}{\theta_0}\right)\right)\Gamma\left(M, \frac{T_h}{\theta_0}\right) \end{aligned} \tag{26}$$

and

$$\begin{aligned} p_m &= \frac{(1 - \Lambda_1)^2 + \Lambda_1^2}{2} \\ &= \frac{\left(1 - \Gamma\left(M, \frac{T_h}{\theta_1}\right)\right)^2 + \Gamma\left(M, \frac{T_h}{\theta_1}\right)^2}{2}. \end{aligned} \tag{27}$$

B. System Throughput

To analyze the throughput performance of the proposed MAC protocol, an enhanced 3-D discrete-time Markov model has been constructed in Fig. 6, which is different from the typical 2-D Markov model in [37]. The proposed Markov model not only depicts the backoff procedure but also depicts the EH procedure. In Fig. 6, we set $\delta = W$ as an example, which leads to the synchronized decrease of the traditional backoff counter and the EH timer δ [e.g., the state transits from (0, 1, 1) to (0, 0, 0) at the same time]. In fact, the EH timer δ can be randomly selected, i.e., $\delta \in [0, W_s - 1]$. The state of the ith BD is denoted as (s, W, δ), where $s \in [0, m]$, $W \in [0, W_s - 1]$, and $\delta = W \in [0, W_s - 1]$ denote the backoff stage, the backoff counter, and the EH time, respectively. Each BD is assumed with the saturation traffic, and then we can get

$$\begin{cases} P_{s,W,\delta|s,W,\delta} = p_{\text{Busy}} & W \in [0, W_s - 1],\ s \in [0, m] \\ P_{s,W,\delta|s,W+1,\delta+1} = p_{\text{Idle}} & W \in [0, W_s - 2],\ s \in [0, m] \\ P_{0,W,\delta|s,0,0} = (1 - p_c)/W_0 & W \in [0, W_0 - 1],\ s \in [0, m] \\ P_{s,W,\delta|s-1,0,0} = p_c/W_s & W \in [0, W_s - 1],\ s \in [1, m] \\ P_{m,W,\delta|m,0,0} = p_c/W_m & W \in [0, W_m - 1], s = m \end{cases} \tag{28}$$

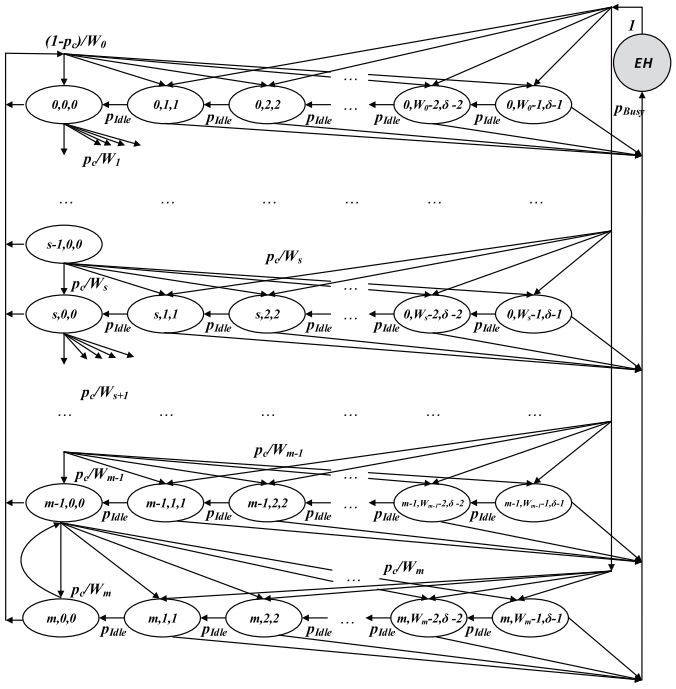

Fig. 6. Three-dimensional discrete Markov model, where we set $\delta = W_s$ as an example.

where p_c is the probability that a collision happen while the ith BD transmission, and $W_s = 2^s W_0$ is the contention window when backoff stage is s, and W_0 denotes the minimum contention window. The first expression in (28) means that the backoff counter is suspended and the ith BD starts the EH of the duration of δ with probability p_{Busy} (i.e., a probability that the channel is sensed to be busy). The second expression is shown that the backoff counter (W) and the EH time (δ) are decremented one slot with probability P_{Idle} (i.e., a probability that the channel is sensed to be idle). The third expression is explained that a new packet following a successful packet transmission begins the backoff with "$s = 0$," and thus the backoff counter and the EH time are reset in the range $[0, W_0 - 1]$. The remaining cases model the system after an unsuccessful transmission. Specifically, as considered in the fourth expression in (28), when an unsuccessful transmission occurs at the backoff stage of $s - 1$, the backoff stage will be increased by one (i.e., backoff stage is s), and a new initial backoff counter value and a new initial EH time are uniformly selected in the range $[0, W_s - 1]$. Finally, the fifth expression models the fact that once s equals to the maximum value m, it is not increased in subsequent packet transmissions.

Compared with the work in [37], we add another state (EH) into the 2-D Markov model and consider the channel sensing situation, i.e., the probability of p_{Busy} and p_{Idle}, it is noteworthy that p_{Busy} and p_{Idle} are related to the two types of the sensing errors' probability (p_f and p_m). Based on (28), let $b_{s,W,\delta}$ be the steady probability that the ith BD is in the state of $\{s, W, \delta\}$, then, we can determine the probability τ that the BD transmits packet in a random slot as

$$\tau = \sum_{s=0}^{m} b_{s,0,0}$$

$$= \frac{2(1-2p_c)\left(1-p_{\text{Busy}}\right)}{(1-2p_c)(W_0+1)+p_c W_0(1-(2p_c)^m)} \tag{29}$$

where p_c is a probability that at least one of $N-1$ remaining BDs transmit in a time slot. Thus, at the steady state, we can calculate p_c as

$$p_c = 1 - (1-\tau)^{N-1}. \tag{30}$$

According to the previous discussions relative to the channel sensing results, we know p_{Busy} and p_{Idle} that consist of sensing errors can be denoted as the appeared backscatter signal and the absented backscatter signal, respectively (i.e., $B_l = 1$ and $B_l = 0$). Thus, we can get

$$\begin{aligned} p_{\text{Busy}} &= P(\phi = 1) \\ &= \frac{1}{2}\sum_{\alpha=0}^{1} P(\mathcal{D}_3|\mathfrak{H}_\alpha) + \frac{1}{2}\sum_{\alpha=0}^{1} P(\mathcal{D}_4|\mathfrak{H}_\alpha) \\ &= \frac{P(\mathcal{D}_3|\mathfrak{H}_0) + P(\mathcal{D}_3|\mathfrak{H}_1) + P(\mathcal{D}_4|\mathfrak{H}_0) + P(\mathcal{D}_4|\mathfrak{H}_1)}{2} \end{aligned} \tag{31}$$

and

$$\begin{aligned} p_{\text{Idle}} &= P(\phi = 0) \\ &= \frac{1}{2}\sum_{\alpha=0}^{1} P(\mathcal{D}_1|\mathfrak{H}_\alpha) + \frac{1}{2}\sum_{\alpha=0}^{1} P(\mathcal{D}_2|\mathfrak{H}_\alpha) \\ &= \frac{P(\mathcal{D}_1|\mathfrak{H}_0) + P(\mathcal{D}_1|\mathfrak{H}_1) + P(\mathcal{D}_2|\mathfrak{H}_0) + P(\mathcal{D}_2|\mathfrak{H}_1)}{2}. \end{aligned} \tag{32}$$

From (21), (31), and (32), p_{Busy} and p_{Idle} can be separately calculated as

$$\begin{aligned} p_{\text{Busy}} &= (1-\Lambda_0)\Lambda_0 + (1-\Lambda_1)\Lambda_1 \\ &= \left(1-\Gamma\left(M, \frac{T_h}{\theta_0}\right)\right)\Gamma\left(M, \frac{T_h}{\theta_0}\right) \\ &\quad + \left(1-\Gamma\left(M, \frac{T_h}{\theta_1}\right)\right)\Gamma\left(M, \frac{T_h}{\theta_1}\right) \end{aligned} \tag{33}$$

and

$$\begin{aligned} p_{\text{Idle}} &= \frac{(1-\Lambda_0)^2 + (1-\Lambda_1)^2 + \Lambda_0^2 + \Lambda_1^2}{2} \\ &= \frac{1}{2}\left(\left(1-\Gamma\left(M, \frac{T_h}{\theta_0}\right)\right)^2 + \left(1-\Gamma\left(M, \frac{T_h}{\theta_1}\right)\right)^2\right) \\ &\quad + \frac{1}{2}\left(\Gamma\left(M, \frac{T_h}{\theta_0}\right)^2 + \Gamma\left(M, \frac{T_h}{\theta_1}\right)^2\right). \end{aligned} \tag{34}$$

By jointly using (29), (30), and (33), the value of τ and p_c can be solved.

Let $\mathcal{S}$ be the normalized system throughput that is defined as the successfully transmit payload bits in a unit time. Referring to [37], $\mathcal{S}$ is calculated as

$$\mathcal{S} = \frac{P_s E[P]}{P_e \sigma + P_s T_s + P_c T_c} \tag{35}$$

where $E[P]$ denotes as the average length of the packet payload. T_s, σ, and T_c represent the time of successful transmission, idle state, and collision, respectively. Moreover, P_s, P_e,

and P_c denote as the probability of successful transmission, the probability of idle channel, and the probability of collision, respectively, which are given

$$\begin{cases} P_s = N\tau(1-\tau)^{N-1} \\ P_e = (1-\tau)^N \\ P_c = 1 - P_s - P_e. \end{cases} \tag{36}$$

It is noted that the throughput value can be obtained by specifying the corresponding values T_s and T_c, which can be calculated as in

$$\begin{cases} T_s = T_{H+E[P]} + \text{DIFS} + T_{\text{ACK}} + \text{SIFS} \\ T_c = T_{H+E[P]} + \text{DIFS} \end{cases} \tag{37}$$

where H is the packet header that is composed of the physical header and the MAC header. $T_{H+E[P]}$ denotes the required time for packet transmission. DIFS and SIFS are the duration of DIFS and SIFS, respectively. T_{ACK} is the time for ACK transmission. σ equals one slot.

C. Throughput Maximization

To solve the upper bound of the normalized throughput, (35) is rearranged as

$$\mathcal{S} = \frac{E[p]}{T_s - T_c + \frac{T_c - P_e(T_c - \sigma)}{P_s}}. \tag{38}$$

Due to T_s, T_c, and σ are constants, $\mathcal{S}$ is maximized when the following part is maximized:

$$\frac{P_s}{\frac{T_c}{\sigma} - P_e\left(\frac{T_c}{\sigma} - 1\right)} = \frac{N\tau(1-\tau)^{N-1}}{T_c^* - (1-\tau)^N\left(T_c^* - 1\right)}. \tag{39}$$

Let $T_c^* = (T_c/\sigma)$ denote as the duration of a collision measured in slot units σ, solving a derivative of (39) with respect to τ, and let it equal to zero. After some calculation, we have

$$(1-\tau)^N - T_c^*\left(N\tau - \left(1 - (1-\tau)^N\right)\right) = 0. \tag{40}$$

When $\tau \ll 1$

$$(1-\tau)^N = 1 - N\tau + \frac{1}{2}N(N-1)\tau^2 \tag{41}$$

and thus an approximate solution of τ can be obtained as

$$\tau \approx \frac{1}{N\sqrt{\frac{T_c^*}{2}}}. \tag{42}$$

From (29) and (30), it is shown that τ depends on the network size N, the system parameters (m, W_m), and the detection threshold T_h. It is known that N is a random variable, hence, given the estimated value of N, we can maximize the throughput performance by optimizing the values (m, W_m) and T_h which consequent to τ.

Furthermore, we derive the value of p_{Busy} based on (33). It is assumed that the parameters (m, W_m) are given as constants (i.e., $m = 0$, $W_m = W_0$). In this case, we discuss the optimization problem of T_h as follows.

According to (29), τ can be rewritten as

$$\tau = \frac{2\left(1 - p_{\text{Busy}}\right)}{1 + W_0}. \tag{43}$$

TABLE I
SIMULATION PARAMETERS

Parameter	Value
The number of samples (M)	50
Energy harvesting rate	1 μW
Transmitted power	0.25 μW
Received power	0.52 μW
W_0	15
W_m	1023
SIFS	10 μs
DIFS	50 μs
σ	20 μs

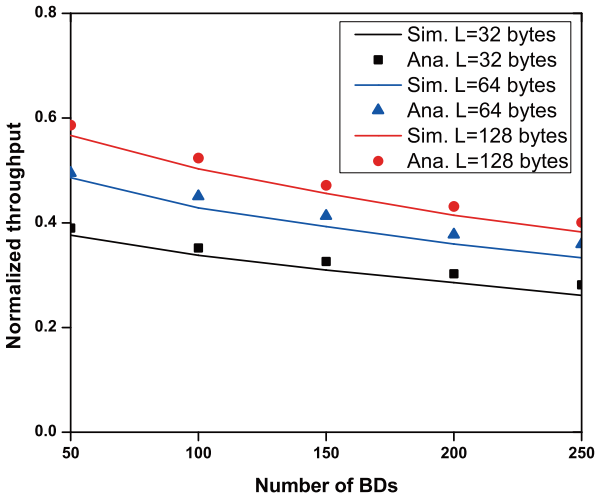

Fig. 7. Normalized throughput versus number of BDs.

Combined with (42), to maximize the system throughput, the optimal probability that channel is sensed to be busy (p_{Busy}^*) is calculated as

$$p_{\text{Busy}}^* = 1 - \frac{1 + W_0}{2N\sqrt{\frac{T_c^*}{2}}}. \tag{44}$$

By substituting (44) into (33), an optimal detection threshold can be derived accordingly.

V. NUMERICAL RESULTS

It is supposed that in the backscatter communication system, the RF source is the continuous signal and each BD generates the saturation traffic. Furthermore, each BD is deployed within the range of each other, it means that each BD can hear each other. Besides, the Rayleigh fading channel is assumed due to the non-line-of-sight (NLOS) scenario is considered. For simplicity, we ignore the difference of the channel between the ambient source and different BDs, and the difference between different BDs. The simulation is performed using NS-2 simulator [38], and then some critical simulation parameters are listed in Table I. Besides, we use the abbreviation sim. and ana. to indicate the simulation result and analysis result, respectively.

A. Performance Evaluation of Normalized Throughput

In Fig. 7, the analysis results and simulation results of normalized throughput are presented with different payload size.

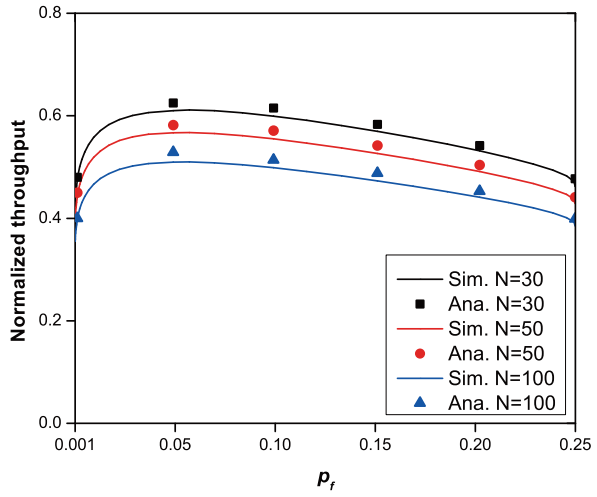

Fig. 8. Normalized throughput versus p_f, where $L = 128$ bytes.

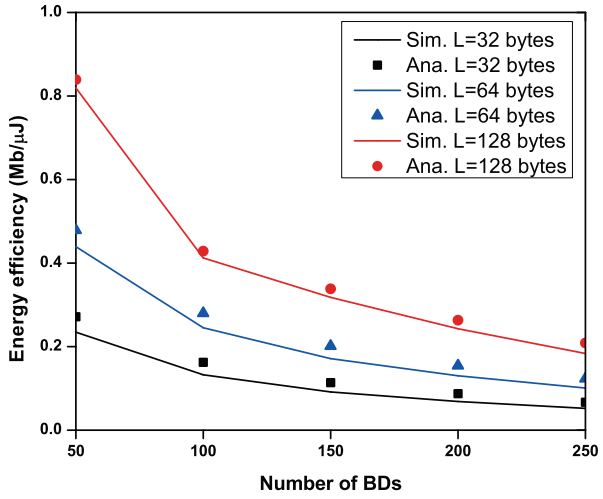

Fig. 10. Energy efficiency versus the number of BDs.

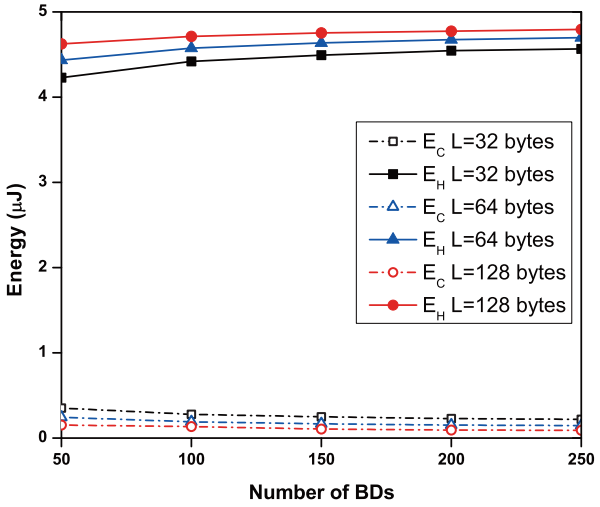

Fig. 9. Consumed energy and harvested energy versus the number of BDs.

On the one hand, it can be seen that the normalized throughput analysis is well verified by the simulation results. On the other hand, when the number of BDs increases, the normalized throughput performance shows a slight decline owning that the more collisions are incurred. Besides, a straightforward phenomenon can be shown that the larger the data packet, the better throughput performance can be obtained. That means more duration can be used for one valid packet transmission through one random competition, thereby decreasing the total time length of the competition process.

The effect of the probability of false alarm (p_f) to the normalized throughput is evaluated in Fig. 8, where the data payload size is set to be $L = 128$ bytes. An optimal threshold is obtained when $p_f = 0.05$ to minimize p_m and maximize the throughput. As the threshold is less than the optimal threshold, with an increase of p_f, it is observed that the normalized throughput increases first due to the large declining of p_m. The normalized throughput is maximized when the threshold reaches the optimal threshold. As the threshold larger than the optimal threshold, the throughput decreases with the increase of p_f and p_m.

B. Performance Evaluation of Energy Harvesting

Fig. 9 depicts the variation tendency of the consumed energy and the harvested energy according to the number of BDs, where we assume that there always exists a continuous ambient signal, and the payload size (L) of each BD transmitter is 32, 64, and 128 bytes, respectively. E_c denotes the consumed energy of one required BD and E_H is the harvested energy of one BD from the RF source. As the number of BDs increases, we can see that E_H monotonically increases while E_c decreases with different data packet length. This is because the more the BDs try to access the channel, the more collision will occur. In this case, the probability of the channel becoming busy increases, so each BD except the current communication BD pair can obtain more time to harvest energy. It is noteworthy that with increasing the data payload size, E_H can be improved but E_C is decreased. This is because the current larger packet transmission will bring more time to harvest energy for other BDs. In contrast, the BD has a fewer chance to transmit the larger packet due to the "long collision" problem, therefore, the consumed energy of the BD decreases, which directly results in the more duration of the channel is sensed to be busy.

It should be noted that the results in Fig. 9 in the original manuscript are achieved under an ideal case where we assume that there always exists a continuous ambient signal. In practice, the scenarios with the semi-passive BDs and discrete ambient signal may occur sometimes. In this case, the ambient backscatter communications cannot be initiated by the BDs without the ambient signals, unless with the help of the traditional RF transmission and hardware circuit operations initiated by themselves. Considering that the energy consumption of data transmission is generally far larger than that of receiving and sensing, therefore, the saved energy may still be drained in this kind of scenario with hybrid ambient signals.

Fig. 10 demonstrates energy efficiency versus the number of BDs with different payload size. Referring to the general definition of energy efficiency given in the existing works [33], [39], [40], in this article, the energy efficiency (ξ) is defined as a ratio of the total achieved throughput to

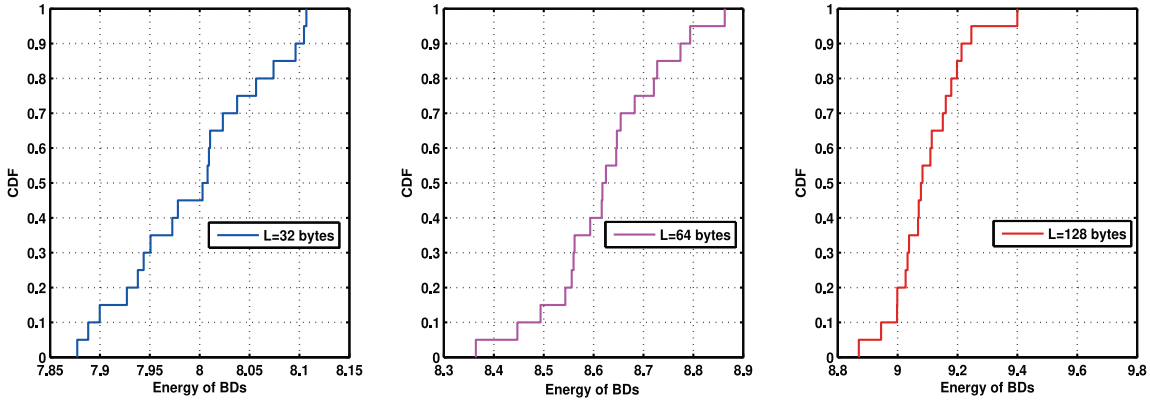

Fig. 11. CDF curve of BDs' energy, the operation time is set as 10 s and $N = 40$.

the consumed energy, i.e., $\xi = (\text{Thr}/\sum E_C)$, where Thr and $\sum E_C$ denotes the achieved system throughput and the overall energy consumption, respectively. Therefore, a larger system throughput or smaller energy consumption can result in larger energy efficiency. Specifically, it is observed from Fig. 10 that the simulation results validate the analysis results. Besides, we can see that the more deployed BDs, the smaller ξ is achieved. The main reason is that due to the inherent limitation of the contention-based random access, the proportion of time suffering collisions increases with the increase of the number of BDs, which leads to the low system throughput and also brings a large energy consumption. Therefore, the energy efficiency ξ significantly decreases accordingly.

Fig. 11 shows the cumulative distribution function curve of BDs' remaining energy. First, we can observe the changing of CDF curve from three subfigures when the data packet payload size is fixed, i.e., $L = 32$ bytes, $L = 64$ bytes, and $L = 128$ bytes. In each subfigure, each BD's remaining energy concentrates in a fairly small range (e.g., less than 0.5 μW gaps). This common phenomenon illustrates that the remaining energy of each BD is very close to each other, and it is demonstrated each BD can efficiently perform the EH in the proposed MAC protocol. Besides, when the data payload size increases, it can be seen that the remaining energy of each BD can be improved when each BD has been set the same initial power. All these benefits that have been revealed can show that the proposed distributed MAC protocol for backscatter communication can obtain an outstanding performance in terms of the EH in the dense deployment scenarios, like IoT.

C. Performance Evaluation of the Dual-Backoff Scheme

In order to evaluate the performance of the dual-backoff scheme, first, three benchmark backoff schemes are defined as follows.

1) *Typical Backoff With Fixed δ:* δ is fixed before each data transmission, and δ will be reselected until the current data transmission is finished.
2) *Typical Backoff With Random δ:* δ is randomly selected for each EH procedure.
3) *Typical Backoff Without δ:* i.e., $\delta = 0$.

The contention overhead can be defined as the sum of the backoff time (i.e., the channel is idle) and the EH time (i.e., the channel is busy) before each data transmission. Compared to the proposed dual-backoff scheme where the EH period (with δ time slots) is decreased gradually, on one the hand, if δ is fixed before each data transmission, the BD usually spends more time on the EH before the data transmission. It can be inferred that the data transmission cannot even be initiated even when the channel has already become idle in this case. This is because the fixed EH has not finished yet. On the other hand, if δ is randomly selected for each EH procedure, the average length of δ will usually be higher than δ using the dual-backoff scheme. From the point of long-term, the computation overhead $\mathcal{O}_d$ of the dual-backoff scheme is bigger than ($\mathcal{O}_n$) that is without δ, and is less than both of ($\mathcal{O}_f$) using the fixed δ as well as $\mathcal{O}_r$ with randomly selecting of δ, i.e., $\mathcal{O}_n < \mathcal{O}_d < \min(\mathcal{O}_f, \mathcal{O}_r)$.

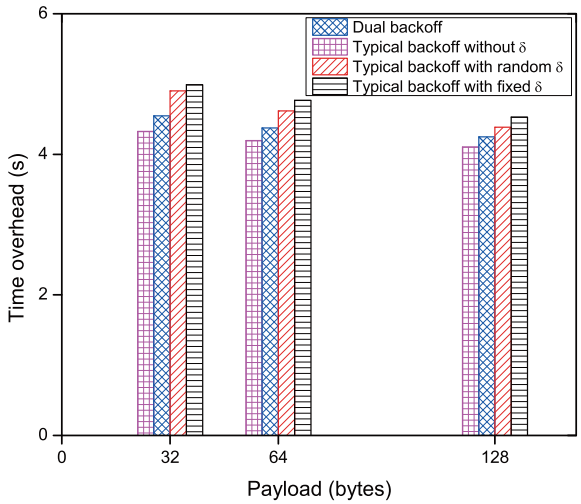

Fig. 12. Time overhead versus payload using the different scheme, where the data payload is set to be $L = 32$ bytes, $L = 64$ bytes, and $L = 128$ bytes, respectively.

We perform the simulations to compare the contention overhead of the proposed dual-backoff scheme with three benchmark schemes (i.e., randomly selecting of δ, fixed δ and without δ), where the data payload is set to be $L = 32$ bytes, $L = 64$ bytes, and $L = 128$ bytes, respectively, as shown in Fig. 12. We can observe from Fig. 12 that the proposed dual-backoff-based MAC protocol outperforms the backoff schemes

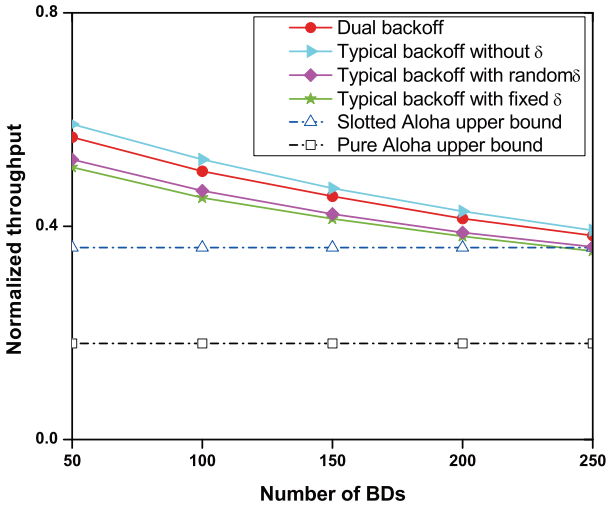

Fig. 13. Normalized throughput versus the number of BDs using the different scheme, where $L = 128$ bytes.

with randomly selecting of δ and fixed δ. This is because δ can be also dynamically decreased in the proposed dual-backoff scheme to prevent BDs from staying in the Harvesting sub-state for a long time. Moreover, it is observed that the backoff scheme without δ achieves the lowest overhead due to no time cost in EH (i.e., the backoff scheme without δ cannot harvest energy).

Furthermore, we evaluate the throughput of the proposed dual-backoff-based MAC protocol and compare with the three benchmark backoff schemes, the upper bound of the pure Aloha and slotted Aloha protocols (i.e., the channel utilization of pure Aloha and slotted Aloha can be at most 18% and 36%, respectively, [41]), as illustrated in Fig. 13. Contrary to the overhead given in Fig. 12, it can be seen from Fig. 13 that the throughput of the proposed dual-backoff scheme outperforms other schemes except for the backoff without δ, in which no extra time cost is spent to harvest energy.

VI. Conclusion

In this article, we proposed a distributed MAC protocol in the ambient backscatter communication system for IoT networks, which enables each BD to switch freely among the backscatter transmission, receiving, and EH in a distributed way. Moreover, an ultralow-power sensing scheme and the dual-backoff mechanism were adopted in the proposed MAC protocol. With the consideration of the sensing errors (i.e., false alarm and miss detection), an enhanced 3-D discrete Markov chain model including EH was presented to analyze the normalized throughput of the proposed MAC protocol. Besides, the upper bound of the normalized throughput was derived with an optimal comparator threshold. The numerical results show that the proposed MAC protocol operates well under the strict low-power consumption for IoT networks.

References

[1] C. Zhu, V. C. M. Leung, L. Shu, and E. C.-H. Ngai, "Green Internet of Things for smart world," *IEEE Access*, vol. 3, pp. 2151–2162, 2015.

[2] V. C. M. Leung, F. R. Yu, and X. Zhang, *Green Communications and Networking*. New York, NY, USA: CRC Press, Apr. 2016.

[3] D. T. Hoang, D. Niyato, P. Wang, D. I. Kim, and Z. Han, "Ambient backscatter: A new approach to improve network performance for RF-powered cognitive radio networks," *IEEE Trans. Commun.*, vol. 65, no. 9, pp. 3659–3674, Sep. 2017.

[4] D. T. Hoang, D. Niyato, P. Wang, D. I. Kim, and L. B. Le, "Overlay RF-powered backscatter cognitive radio networks: A game theoretic approach," in *Proc. ICC*, Paris, France, May 2017, pp. 1–6.

[5] D. T. Hoang, D. Niyato, P. Wang, D. I. Kim, and L. B. Le, "Optimal data scheduling and admission control for backscatter sensor networks," *IEEE Trans. Commun.*, vol. 65, no. 5, pp. 2062–2077, May 2017.

[6] X. Lu, H. Jiang, D. Niyato, D. I. Kim, and Z. Han, "Wireless-powered device-to-device communications with ambient backscattering: Performance modeling and analysis," *IEEE Trans. Wireless Commun.*, vol. 17, no. 3, pp. 1528–1544, Mar. 2018.

[7] X. Lu, D. Niyato, H. Jiang, D. I. Kim, Y. Xiao, and Z. Han, "Ambient backscatter assisted wireless powered communications," *IEEE Wireless Commun.*, vol. 25, no. 2, pp. 170–177, Apr. 2018.

[8] P. Kamalinejad, K. Keikhosravy, R. Molavi, S. Mirabbasi, and V. C. M. Leung, "An ultra-low-power CMOS voltage-controlled ring oscillator for passive RFID tags," in *Proc. New Circuits Syst. Conf. (NEWCAS)*, Jun. 2014, pp. 456–459.

[9] C. He, Z. J. Wang, C. Miao, and V. C. M. Leung, "Block-level unitary query: Enabling orthogonal-like space-time code with query diversity for MIMO backscatter RFID," *IEEE Trans. Wireless Commun.*, vol. 15, no. 3, pp. 1937–1949, Mar. 2016.

[10] C. He, Z. J. Wang, and V. C. M. Leung, "Unitary query for the $M \times L \times N$ MIMO backscatter RFID channel," *IEEE Trans. Wireless Commun.*, vol. 14 no. 5, pp. 2613–2625, May 2015.

[11] N. Van Huynh, D. T. Hoang, X. Lu, D. Niyato, P. Wang, and D. I. Kim, "Ambient backscatter communications: A contemporary survey," *IEEE Commun. Surveys Tuts.*, to be published.

[12] W. Liu, K. Huang, X. Zhou, and S. Durrani, "Next generation backscatter communication: Systems, techniques, and applications," *EURASIP J. Wireless Commun. Netw.*, vol. 2019, no. 1, pp. 1–11, Dec. 2019.

[13] J. Kimionis, A. Bletsas, and J. N. Sahalos, "Bistatic backscatter radio for power-limited sensor networks," in *Proc. GLOBECOM*, Atlanta, GA, USA, Dec. 2013, pp. 353–358.

[14] G. Yang and Y.-C. Liang, "Backscatter communications over ambient OFDM signals: Transceiver design and performance analysis," in *Proc. GLOBECOM*, Washington, DC, USA, Dec. 2016, pp. 1–6.

[15] G. Yang, Y.-C. Liang, R. Zhang, and Y. Pei, "Modulation in the air: Backscatter communication over ambient OFDM carrier," *IEEE Trans. Commun.*, vol. 66, no. 3, pp. 1219–1233, Mar. 2018.

[16] G. Yang, D. Yuan, Y. C. Liang, R. Zhang, and V. C. M. Leung, "Optimal resource allocation in full-duplex ambient backscatter communication networks for wireless-powered IoT," *IEEE Internet Things J.*, vol. 6, no. 2, pp. 2612–2625, Apr. 2019.

[17] W. Liu, K. Huang, X. Zhou, and S. Durrani, "Time-hopping multiple-access for backscatter interference networks," in *Proc. GLOBECOM*, Singapore, Dec. 2017, pp. 1–7.

[18] W. Liu, Y. C. Liang, Y. Li, and B. Vucetic, "Backscatter multiplicative multiple-access systems: Fundamental limits and practical design," *IEEE Trans. Wireless Commun.*, vol. 17, no. 9, pp. 5713–5728, Sep. 2018.

[19] D. T. Hoang, D. Niyato, P. Wang, D. I. Kim, and L. B. Le, "Overlay RF-powered backscatter cognitive radio networks," in *Proc. IEEE ICC*, Paris, France, May 2017, pp. 1–6.

[20] S. H. Kim and D. I. Kim, "Hybrid backscatter communication for wireless-powered heterogeneous networks," *IEEE Trans. Wireless Commun.*, vol. 16, no. 10, pp. 6557–6570, Oct. 2017.

[21] D. T. Hoang, D. Niyato, P. Wang, D. I. Kim, and Z. Han, "The tradeoff analysis in RF-powered backscatter cognitive radio networks," in *Proc. IEEE GLOBALCOM*, Washington, DC, USA, Dec. 2016, pp. 1–6.

[22] G. Khandelwal, K. Lee, A. Yener, and S. Serbetli, "ASAP: A MAC protocol for dense and time-constrained RFID systems," *EURASIP J. Wireless Commun. Netw.*, vol. 2007, no. 2, p. 3, Jan. 2007.

[23] J. Haapola, L. Goratti, I. Suliman, and A. Rabbachin, "Preamble sense multiple access (PSMA) for impulse radio ultra wideband sensor networks," in *Proc. Int. Workshop Embedded Comput. Syst.*, Jul. 2006, pp. 155–166.

[24] A. N. Parks, A. P. Sample, Y. Zhao, and J. R Smith, "A wireless sensing platform utilizing ambient RF energy," in *Proc. IEEE Power Amplifiers Wireless Radio Appl. (PAWR)*, Austin, TX, USA, Jan. 2013, pp. 160–162.

[25] B. Kellogg, A. N. Parks, S. Gollakota, J. R. Smith, and D. Wetherall, "Wi-Fi backscatter: Internet connectivity for RF-powered devices," in *Proc. ACM SIGCOMM*, Chicago, IL, USA, Aug. 2014, pp. 607–618.

[26] B. Kellogg, V. Talla, S. Gollakota, and J. R. Smith, "Passive Wi-Fi: Bringing low power to Wi-Fi transmissions," in *Proc. NSDI*, Santa Clara, CA, USA, Mar. 2016, pp. 151–164.

[27] V. Liu, A. N. Parks, V. Talla, S. Gollakota, D. Wetherall, and J. R. Smith, "Ambient backscatter: Wireless communication out of thin air," in *Proc. ACM SIGCOMM*, Hong Kong, Aug. 2013, pp. 39–50.
[28] Z. Ma, L. Feng, and F. Xu, "Design and analysis of a distributed and demand-based backscatter MAC protocol for Internet of Things networks," *IEEE Internet Things J.*, vol. 6, no. 1, pp. 1246–1256, Feb. 2009.
[29] M. A. ElMossallamy, Z. Han, M. Pan, R. Jantti, K. G. Seddik, and G. Y. Li, "Backscatter communications over ambient OFDM signals using null subcarriers," in *Proc. IEEE GLOBECOM*, Abu Dhabi, UAE, Dec. 2018, pp. 1–6.
[30] A. N. Parks, A. P. Sample, Y. Zhao, and J. R. Smith, "A wireless sensing platform utilizing ambient RF energy," in *Proc. IEEE Topical Conf. Biomed. Wireless Technol. Netw. Sensing Syst.*, Austin, TX, USA, Jan. 2013, pp. 154–156.
[31] H. Nishimoto, Y. Kawahara, and T. Asami, "Prototype implementation of ambient RF energy harvesting wireless sensor networks," in *Proc. IEEE Conf. Sensors*, Nov. 2010, pp. 1282–1287.
[32] P. Zhang and D. Ganesan, "Enabling bit-by-bit backscatter communication in severe energy harvesting environments," in *Proc. NSDI*, Apr. 2014, pp. 345–357.
[33] X. Lu, P. Wang, D. Niyato, D. I. Kim, and Z. Han, "Wireless networks with RF energy harvesting: A contemporary survey," *IEEE Commun. Surveys Tuts.*, vol. 17, no. 2, pp. 757–789, 2nd Quart., 2015.
[34] F. Iannello, O. Simeone, and U. Spagnolini, "Energy management policies for passive RFID sensors with RF-energy harvesting," in *Proc. IEEE ICC*, May 2010, pp. 1–6.
[35] X. Li, X. Wang, P.-J. Wan, Z. Han, and V. C. M. Leung, "Hierarchical edge caching in device-to-device aided mobile networks: Modeling, optimization, and design," *IEEE J. Sel. Areas Commun.*, vol. 36, no. 8, pp. 1768–1785, Aug. 2018.
[36] D. Darsena, G. Gelli, and F. Verde, "Modeling and performance analysis of wireless networks with ambient backscatter devices," *IEEE Trans. Commun.*, vol. 65, no. 4, pp. 1797–1814, Apr. 2017.
[37] G. Bianchi, "Performance analysis of the IEEE 802.11 distributed coordination function," *IEEE J. Sel. Areas Commun.*, vol. 18, no. 3, pp. 535–547, Mar. 2000.
[38] *NS-2 Network Simulator*. [Online]. Available: https://www.isi.edu/nsnam/ns/
[39] J. Wang, H. Hassanieh, D. Katabi, and P. Indyk, "Efficient and reliable low-power backscatter networks," in *Proc. ACM SIGCOMM*, Helsinki, Finland, Aug. 2012, pp. 61–72.
[40] D. W. K. Ng, E. S. Lo, and R. Schober. "Energy-efficient power allocation in OFDM systems with wireless information and power transfer," in *Proc. IEEE ICC*, Budapest, Budapest, Jun. 2013, pp. 4125–4130.
[41] G. Jie. (2007). *Analysis of Aloha and Slotted Aloha*. [Online]. Available: https://www3.cs.stonybrook.edu/~jgao/CSE370-spring07/aloha-analysis.pdf

Xuelin Cao (S'19) received the M.S. degree in information and signal processing and the Ph.D. degree in information and communication engineering from Northwestern Polytechnical University (NPU), Xi'an, China, in 2010 and 2019, respectively.

From 2010 to 2012, she worked as an Engineer with the CDMA BTS Lab, Nokia Siemens Networks, Hangzhou, China. She has been a Visiting Scholar with the Department of ECE, University of Houston, Houston, TX, USA, since 2017. Her research interests include MAC protocol design and modeling, 5G heterogeneous networks, and backscatter communications.

Zuxun Song received the B.E., M.S., and Ph.D. degrees from Northwestern Polytechnical University (NPU), Xi'an, China, in 1986, 1989, and 2004, respectively.

He is currently a Research Fellow of 365 Research Institute, NPU. His research interests are in the area of UAV data link, electromagnetic compatibility, microwave communication, electronic system simulation. He has presided over and participated in the research projects, including national defense 973, national 863, and national defense technology foundation.

Dr. Song is currently the Vice Chairman of EMC Technical Committee of Shaanxi Institute of Electronics, and a member of the EMC Technical Committee of China Institute of Industry, Remote Sensing, and Telemetry and Remote-Control Branch of China Institute of Electronics.

Bo Yang (M'19) received the B.E., M.S., and Ph.D. degrees from Northwestern Polytechnical University, Xi'an, China, in 2007, 2010, and 2016, respectively.

He is currently a Postdoctoral Fellow with the Department of Electrical and Computer Engineering, Prairie View A&M University, and a member of the Texas A&M University System, Prairie View, TX, USA. He chaired the Session titled "Machine Learning in IoT, M2M, Sensor Networks, and Ad-Hoc Networking" in IEEE VTC-Fall 2018. His current research focuses on machine learning, MAC design for IoT, and application of AI for wireless networks.

Mohamed A. ElMossallamy (S'14) received the M.Sc. degree in electronics and communications engineering from American University in Cairo, Cairo, Egypt, in 2017. He is currently pursuing the Ph.D. degree with the Department of Electrical and Computer Engineering, University of Houston, Houston, TX, USA.

His current research interests include transceiver design and performance analysis for the Internet of Things, massive MIMO-OFDM systems, and machine learning for wireless communications.

Lijun Qian (SM'08) received the B.S. degree from Tsinghua University, Beijing, China, the M.S. degree from the Technion—Israel Institute of Technology, Haifa, Israel, and the Ph.D. degree from Rutgers University, Newark, NJ, USA.

He was a Technical Staff Member of Bell-Labs Research, Murray Hill, NJ, USA. He is a Regents Professor and holds the AT&T Endowment with the Department of Electrical and Computer Engineering, Prairie View A&M University, Prairie View, TX, USA, and a member of the Texas A&M University System, Houston, TX, USA, where he is also the Director of the U.S. DOD Center of Excellence in Research and Education for Big Military Data Intelligence (CREDIT Center). He is a Visiting Professor with Aalto University, Espoo, Finland. His research interests are in the area of big data processing, artificial intelligence, wireless communications and mobile networks, network security and intrusion detection, and computational and systems biology.

Zhu Han (S'01–M'04–SM'09–F'14) received the B.S. degree in electronic engineering from Tsinghua University, Beijing, China, in 1997, and the M.S. and Ph.D. degrees in electrical and computer engineering from the University of Maryland, College Park, MD, USA, in 1999 and 2003, respectively.

From 2000 to 2002, he was an R&D Engineer of JDSU, Germantown, MD, USA. From 2003 to 2006, he was a Research Associate with the University of Maryland. From 2006 to 2008, he was an Assistant Professor with Boise State University, Boise, ID, USA. He is currently a John and Rebecca Moores Professor with the Electrical and Computer Engineering Department as well as in the Computer Science Department, University of Houston, Houston, TX, USA. He is also a Chair Professor with National Chiao Tung University, Hsinchu, Taiwan. His research interests include wireless resource allocation and management, wireless communications and networking, game theory, big data analysis, security, and smart grid.

Dr. Han has been 1% Highly Cited Researcher by Web of Science since 2017. He received the NSF Career Award in 2010, the Fred W. Ellersick Prize of the IEEE Communication Society in 2011, the EURASIP Best Paper Award for the *Journal on Advances in Signal Processing* in 2015, the IEEE Leonard G. Abraham Prize in the field of Communications Systems (Best Paper Award in the IEEE JOURNAL ON SELECTED AREAS IN COMMUNICATIONS) in 2016, and several best paper awards in IEEE conferences. He was an IEEE Communications Society Distinguished Lecturer from 2015 to 2018. He has been an AAAS Fellow since 2019 and an ACM distinguished member since 2019.